Progress in Organic Coatings 138 (2020) 105428

Contents lists available at ScienceDirect

Progress in Organic Coatings

journal homepage: www.elsevier.com/locate/porgcoat

Hybrid sol–gel coatings doped with cerium nanocontainers for active corrosion protection of AA2024

Thu Thuy Thai[a,b], Anh Truc Trinh[a], Marie-Georges Olivier[b,*]

[a] Laboratory for Protective Coatings, Institute for Tropical Technology, VAST, 18 Hoang Quoc Viet, Hanoi, Viet Nam
[b] Materials Science Department, University of Mons, 20 Place du Parc, 7000 Mons, Belgium

ARTICLE INFO

Keywords:
Sol–gel coating
AA2024
Corrosion
Montmorillonite
Cerium salts
EIS

ABSTRACT

This work presents a new approach to develop protective pre-treatment for AA2024 based on the inhibitor efficiency of cerium ions which are considered as a promising alternative to replace chromate compounds. The inhibition properties of cerium salts for improving the anti-corrosion performance of AA2024 have been characterized by polarization curves and EIS measurements. Cerium ions were inserted into nanoclays platelets by cationic-exchange reactions (CeMMT). XRD analysis proved the presence of cerium ions intercalated into clay structure. EIS measurements and polarization curves highlighted a high corrosion inhibition effect of cerium-modified nanoclays. This effectiveness can be related to the release of 60% of cerium ions from CeMMT structure in sodium chloride as determined by UV–vis measurements. Salt spray test made on scratched sol–gel samples indicated a self-healing effect of cerium ions which provide an active corrosion protection to aluminum substrate. EIS measurements revealed that hybrid sol–gel films doped with CeMMT improve barrier properties and anticorrosion protection of aluminum 2024 substrate.

1. Introduction

Chromated-based compounds are considered as the most efficient inhibitors for the corrosion protection of aluminum alloys substrates due to their low solubility, oxidizing and self-healing abilities [1]. Unfortunately, as chromate (VI) compounds also act as cancerogenic elements for human health and toxic species for environment, alternative inhibitors must be developed in order to obtain an equivalent or higher effectiveness and replace the use of Cr (VI) [1,2].

Among the potential chromate-free inhibitors, cerium-based compounds have been proved to provide an active protection to metallic substrates [3,4]. Their inhibition effect is based on the formation of insoluble hydroxides on the cathodic zones in case of corrosion that block the cathodic reaction and so reduce the global corrosion current rate [3]. Cerium-based inhibitors can be directly incorporated into sol–gel coatings or indirectly by their incorporation in nanocontainers [5–7].

In literature, many studies focused on the use of cerium-based inhibitors doped silane coating as they can improve the barrier properties and the corrosion resistance of the film [5,7–10]. Montemor et al. showed that cerium-based inhibitors can contribute to reduce the porosity of the film, probably by blocking small defects /or cracks in the film structure, [11]. Furthermore, the addition of the cerium compounds can contribute to a good densification due to the formation of Si—O—Ce bonding into silane network [12–15] without increasing the thickness of sol–gel layer [13]. Druart et al showed that the addition of a high concentration of cerium salt (1000 ppm) into sol–gel formulation can reduce the film resistance and provoke the deterioration of silane layer [13]. A concentration of 500 ppm of Ce (III) salt doped in silane layer improved the barrier properties and the resistance in wet atmosphere [13]. In addition, their anti-corrosion properties can also be improved by the self-healing effect due to the incorporation of cerium compounds. According to Palanivel et al., this mechanism can be explained by two different oxidation states of cerium ions: Ce^{3+} and Ce^{4+} [16]. When the cathodic reactions started, the Ce^{3+} ions in the silane film were oxidized to Ce^{4+}, which are more soluble and would then be released from the coating and favorized to the formation of a hydroxide/oxide layer that would protect the metallic substrate.

Nevertheless, the release of inhibitors from the coating in the corrosive solution sometimes is difficult to control, resulting to a rapid consumption of incorporated inhibitors and the formation of osmotic blistering in sol–gel films [7,9]. In some particular cases, the amount of added inhibitor is limited by its solubility, its dispersion in the matrix or its compatibility with the coating [17,18]. In order to solve these difficulties and to assure the self-healing effect, the micro- or nano-particles were useful as containers of inhibitors [6,7,19–21].

* Corresponding author.
E-mail address: marjorie.olivier@umons.ac.be (M.-G. Olivier).

https://doi.org/10.1016/j.porgcoat.2019.105428
Received 5 September 2019; Received in revised form 11 October 2019; Accepted 30 October 2019
Available online 13 November 2019

Sodium montmorillonite (NaMMT) has been well-known as layered silicate clay naturally hydrophilic which contains sodium cations at clay platelets. These defects on its structure give it a negative charge, leading to a high cationic exchange capacity [22–24]. These inorganic ions can be effectively replaced by surfactants, cationic organic molecules by cationic-exchange reactions. In particular, a number of published studies on the use of clay as a container of inhibitors can be found in the literature [6,19,25,26]. Montmorillonite platelets can be dispersed in the polymer binder or sol–gel network by forming intercalated and exfoliated structures which can effectively increase water and aggressive ions diffusion pathways, so consequently improve barrier properties of organic coatings [19,23,25–28]. Motte et al. used cerium (III)-modified montmorillonite incorporated into the silane formulation in order to protect galvanized steel surface [19]. A synergistic effect was found at a concentration of 5000 ppm NaMMT and 100 ppm Ce^{3+}. It was also shown that 4% wt. of NaMMT combined with 2 wt. % cerium nitrate improve the barrier properties of epoxy coating deposited on the carbon steel surface [29]. Moreover, a high concentration of incorporated nanoclays leads to the aggregate formation and an increase of the film porosity, inducing a rapid degradation of the coating [29]. The dispersion of nano-clays must also be optimized when added in coating in order to exploit their platelet structure, leading to good compatibility with the matrix and limiting the formation of aggregates [27,30].

Clay incorporation can improve barrier properties of sol–gel coating. However, the concentration of doped clay was also high, variable from 250 ppm to 5000 ppm or 1% to 5% wt., leading to an increase of film thickness (about few μm) [25,31]. The performance protection of the modified clays is mainly studied on galvanized steel and carbon steel and only few papers are related to the aluminum substrate, especially 2024 aluminum alloy. AA2024 alloy is widely used in aircraft and automobile industry due to its low density and high tensile strength that are achieved by the presence of alloy elements like copper, iron and magnesium [3,18]. Moreover, the formation of micro-galvanic couples into AA2024 alloy structure leads to corrosion processes taking place. So, it needs to develop an effective pretreatment method in order to protect AA2024 alloy [3,21]

In this context, this study focuses on the synthesis of sol–gel coating doped with cerium-modified clay (CeMMT) in order to improve corrosion resistance of 2024AA. Inhibition properties of cerium ions was firstly evaluated by electrochemical impedance spectroscopy and polarization measurements. The cerium-modified clays were then characterized by XRD diffraction, electrochemical measurements, and UV–vis analysis. Sol–gel was formulated by using Tetraethoxysilane (TEOS) and 3-Glycidopropyltrimethoxysilane (GPTMS) as precursors. The NaMMT and CeMMT clays were then incorporated into sol–gel film deposited on aluminum alloy 2024 sample. Anti-corrosion properties of un-doped sol–gel film and clay-doped sol–gel films were then evaluated by electrochemical impedance methods and salt spray test.

2. Method and experiments

2.1. Materials

2.1.1. Aluminum alloy substrate preparation

Aluminum alloy AA2024 (provided by Sonaca company, Belgium) was pretreated depending on the experiment. For the inhibition efficiency test, AA2024 rod (Aludis, France) having a surface area of 1 cm^2 was grinded by SiC abrasive paper with grades from 100 to 1200, rinsed with absolute ethanol, quickly dried before immersion in the studied solution. For the coating evaluation, AA2024 panels with dimension 4 cm × 6 cm × 1 mm were degreased by using acetone, immersed in Turco 4215 solution (10 min, 50 °C), chemically treated in 1 M NaOH (30 s, 40 °C) and Turco Smutgo solution (containing HF, 15 s, room temperature) before application of the sol–gel film.

2.1.2. Cerium-modified clay preparation

The commercial sodium montmorillonite (NaMMT) Cloisite 116® Na (BYK – Southern Clay company) was used. Cerium chloride heptahydrate ($CeCl_3{\cdot}7H_2O$) was purchased from Fluka (99.99%). The amount of 0.5% wt. NaMMT was mixed in demineralized water by stirring for 24 h and then subjected to sonication (30 min, 15 W). These steps favor the exfoliation of the sheets of NaMMT and thus promote the incorporation of the Ce (III) ions by cationic exchange with the Na^+ ions. A quantity of 500 ppm of Ce (III) was then introduced into the clay suspension which was stirred for 24 h. After the modification, cerium-modified clay was collected by centrifugation (Hettich equipment, model Universal 320) at 5000 rpm and rinsed until chloride ions were totally removed. The absence of the chloride trace was verified by using 0.1 M $AgNO_3$ solution. The powder was dried overnight at 80 °C and then manually grinded for the required experiments.

2.1.3. Hybrid sol–gel coating: formulation and deposition conditions

A mix of two different precursors, namely tetraethoxysilane (TEOS, Merck, 99%) and glycidoxypropyltrimethoxysilane (GPTMS, Sigma Aldrich 98%) with ratio molar 1:2 dissolved in a 1:1 (mol ratio) mixture of demineralized water and absolute ethanol was used for sol–gel film. TEOS is used as inorganic precursor in order to improve the thermal and chemical properties of the layer (four hydrolysable functions). It is also available at reasonable price for many applications [13]. GPTMS provides flexibility to the sol–gel network thanks to one non-hydrolysable epoxy group, promotes the coating adhesion and improves the compatibility between AA2024 substrate/sol–gel film and an epoxy coating [32]. Firstly, the amount of NaMMT or CeMMT was ultrasonically dispersed in the demineralized water (30 min, 15 W) then added into sol–gel suspension in order to get finally 0.5% wt. of clay. The pH was setup to 3.5–4 by using 96% acetic acid. After 2 h of hydrolysis time, the sol–gel solution was applied by a KSV Nima Dipcoater (Biolin Scientific) on the pretreated aluminum alloy panels with an immersion time of 2 min, a withdrawal speed of 100 mm/min. After drying for 5 min in air, the plates were dried at 150 °C for 60 min.

2.2. Experiments

2.2.1. Characterization of cerium-modified clay

X-ray diffraction patterns of NaMMT and CeMMT powders were determined by using the XRD D8 ADVANCE equipment with a CuK_α radiation source (1.54065 Å) at room temperature in order to determine the distance between clay platelets. The diffraction was recorded in the range of 1 – 10° with an increment of 0.005°. Zeta potential of NaMMT and CeMMT were determined in demineralized water by using a Zetasizer Nano Series (Malvern).

The quantity of cerium ions released from the modified clay structure was determined by GBC CINTRA 40 Ultra-Visible spectrometry in the region of wavelengths from 200 to 400 nm. Samples of different concentrations of cerium ions (from 10 to 300 ppm) were prepared in 0.1 M NaCl solution. The peaks corresponding to the absorption of Ce (III) were detected and a calibration curve was established. This curve allowed to determine the concentration of Ce (III) released from the modified NaMMT structure versus immersion time in the aggressive solution. Then 1 g of CeMMT was introduced into 500 ml of 0.1 M NaCl solution. A fixed volume (25 ml) of the suspension was taken at different stirring times, then filtered on filter paper and analyzed by UV–vis spectrometer. The measurements were performed at least two times to assure the reproductible results.

2.2.2. Electrochemical measurements

Inhibition properties of cerium (III) ions and CeMMT were characterized using Bio-Logic SP-300 (BioLogic Science Instruments) equipped with a motor EDI 101 (LANGE, Hach) using as rotating electrode (exposed surface area: 1 cm^2). The corrosion protection of sol–gel films and doped sol–gel films deposited onto aluminum 2024

samples were characterized by using Parstat 2273 (Princeton Applied Research) placed in a Faraday cage. The electrolyte solution was 0.1 M NaCl solution and the exposed area was 7.07 cm^2. A three-electrodes system was used, with the differently pretreated AA2024 samples as working electrode, an Ag/AgCl/KCl saturated as reference electrode and a platinum grid as counter electrode. Spectroscopy impedance measurements were performed in a frequency range from 100 kHz to 10 mHz and with 5 mV rms sinusoidal perturbation amplitude at open circuit potential (OCP). Electrochemical parameters were extracted by using ZSim Win 3.50 (Ametek).

The cathodic and anodic branches of the polarization curves were separately determined at a scan rate of 1 mV/s toward a potential value of ± 300 mV starting from the OCP value after 2 h of immersion in the electrolyte solution [33].

2.2.3. Salt pray test

Salt spray test was performed to evaluate the corrosion protection given to AA2024 by the applied sol–gel films. The AA2024 samples covered with the different sol–gel layers were scratched by an artificial defect in the form of a cross of 20 mm × 0.38 mm. The four edges of the aluminum samples were protected by an epoxy paint before exposure. All specimens were then placed in a salt spray test chamber (Q-Fog Cyclic Corrosion Tester, Labomat) according to ASTM B117 standard. After each day of exposure, the samples were removed, rinsed with deionized water and the change of surface appearance was recorded by optical observation equipped with a Leica DFC420 microscope. Film thickness of sol–gel layer was measured on the cross-section with a SEM-FEG Hitachi S-4800.

3. Results and discussions

3.1. Inhibition properties of cerium (III) ions

In this study, 500 ppm of Ce (III) was chosen from the previous study [13] in order to investigate their inhibitive effect on the aluminum alloy by using a AA2024 rotating electrode. The impedance diagrams obtained for AA2024 in 0.1 M NaCl solution with or without inhibitor versus immersion time are presented in the Fig. 1.

Without inhibitor, two time constants are clearly visible: the first one at high frequency is related to the natural aluminum oxide layer at the electrode surface and the second one at low frequency is due to the corrosion processes taking place at the surface [34]. The impedance value obtained at low frequency in this case was low, about $2 \times 10^3\ \Omega\,cm^2$ after 2 h of immersion. In contrast, the impedance modulus values at low frequency obtained for the AA2024 rotating electrode immersed in the sodium chloride solution containing 500 ppm Ce (III) are higher, relatively stable with immersion time and a more capacitive behavior is observed in the middle frequency range due to the protection of the metallic substrate. The impedance modulus value is about an order of magnitude higher compared to one obtained for the reference system. In the presence of inhibitors, only one-time constant is observed from 2 h to 10 h of immersion related to a stable effect of cerium ions at studied concentration for the anticorrosion protection of aluminum 2024. The corrosion processes in the low frequency range are not observed. The second time constant at low frequency only appears after 24 h immersion. In addition, from the impedance diagrams, the inhibition efficiency (I_{eff}) can be calculated following the equation:

$$I_{eff} = \frac{R_p - R_{po}}{R_p} x\ 100\ (\%) \quad (1)$$

where R_p and R_{po} correspond to the polarization resistance values obtained for the measurements with and without corrosion inhibitors. The inhibition efficiency versus immersion time is presented in Table 1. As observed in this table, when the cerium (III) ions are introduced in aerated solution, they display high inhibition properties with an efficiency reaching 95% at the end of the experiment. Fig. 2 shows the images of the AA2024 surface electrode obtained after 2 h of immersion in the electrolyte solution with and without cerium ions. Corrosion products were formed on the surface of the electrode immersed in the reference solution (Fig. 2a) while the electrode surface immersed in the solution containing cerium ions was not corroded (Fig. 2b). These results confirm that cerium (III) ions act as corrosion inhibitor for AA2024 surface. This concentration of cerium ions is then used to be intercalated into the montmorillonite structure.

Table 1
Inhibition efficiency Ieff (%) calculated from impedance measurements versus immersion time in 0.1 M NaCl.

I_{eff} (%)	2 h	4 h	6 h	10 h	24 h
0.1 M NaCl + 500 ppm Ce^{3+}	96.9	97.1	96.9	98	95.1

3.2. Characterization of cerium-modified clay (CeMMT)

X-ray diffraction patterns obtained of the NaMMT and CeMMT are presented in Fig. 3. From the diagrams, using the Bragg's law [23], the calculated interlayer space of the unmodified NaMMT was determined to 12.9 Å. This data is comparable with the measurements reported in the literature [19,22]. On the other hand, the incorporation of cerium into the clay platelets provokes an increase in the d_{001} basal space, which can be observed by an increase of d_{001} value and, also a small displacement of the diffraction peak. The interlayer space obtained for Ce (III) modified-NaMMT is 15.7 Å which can be explained by the interlayer intercalation of the cerium cations (atomic radius = 0.248 nm) characterized by a bigger size than sodium ions (atomic radius = 0.227 nm).

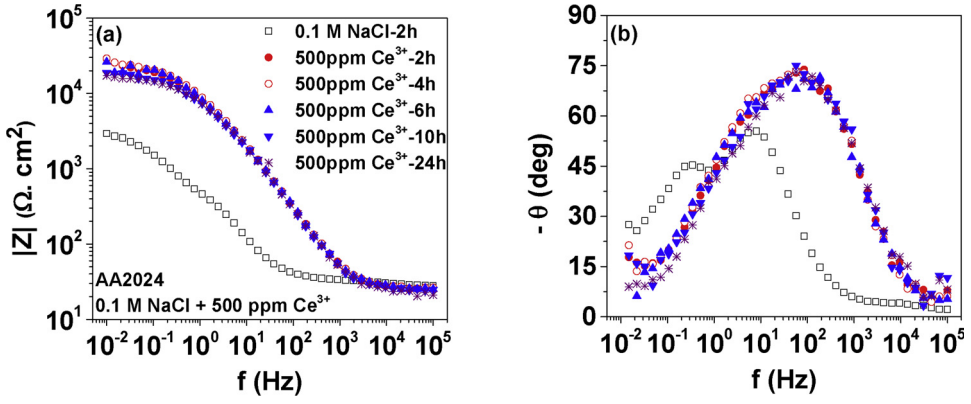

Fig. 1. Bode diagrams of aluminum 2024 rotating electrode versus immersion time in 0.1 M NaCl solution with and without 500 ppm Ce^{3+}.

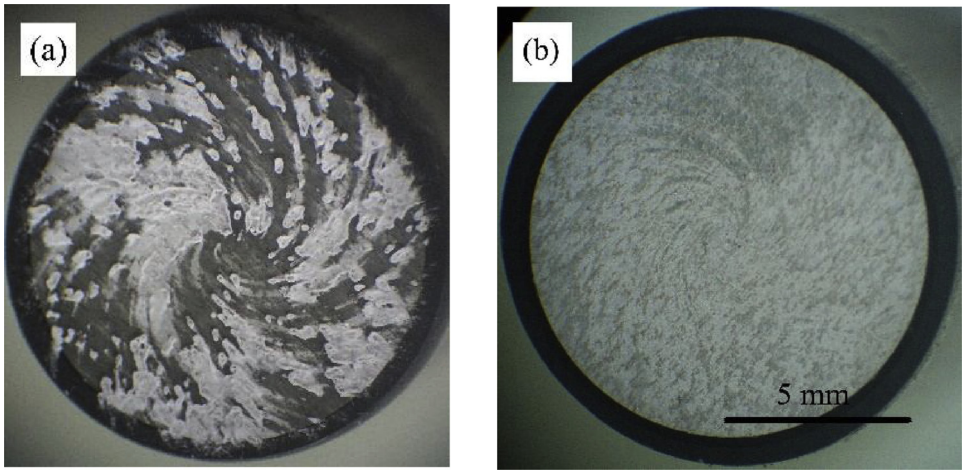

Fig. 2. Optical observations of the surface of AA2024 rotating electrode after 2 h of immersion (a) in 0.1 M NaCl solution, (b) in 0.1 M NaCl solution containing 500 ppm Ce (III).

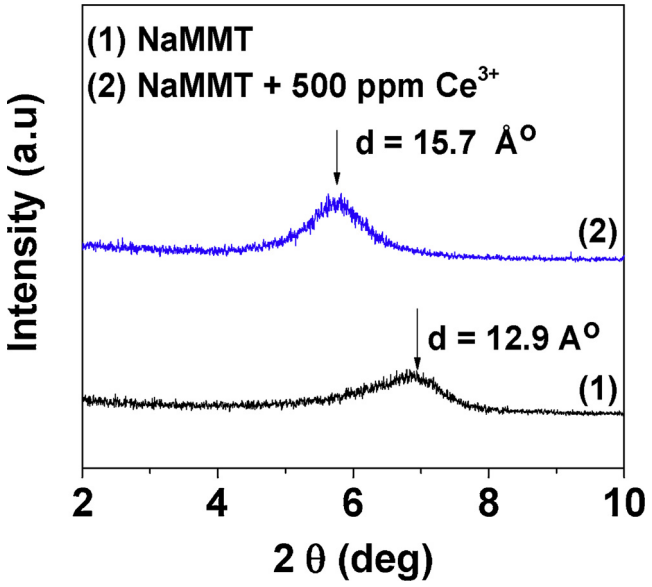

Fig. 3. XRD patterns of unmodifed clay NaMMT and cerium-modified clay CeMMT.

Table 2
Zeta potential values of NaMMT and CeMMT in demineralized water.

Sample	Zeta potential (mV)	pH
NaMMT	−35.9 ± 1.9	10.5
CeMMT	−1.7 ± 0.3	6.2

In addition, Table 2 shows the zeta potential values of the NaMMT and CeMMT determined in demineralized water and, also the pH values of these suspensions. It can be seen that the addition of cerium causes a progressive decrease in the absolute value of the zeta potential and induces a change in pH value: from an alkaline media to a weak acid media. The suspension containing 0.5% wt. cerium-modified clay is less stable due to its low zeta potential value close to 0 mV. This phenomenon can be explained by the compensation of the negative charge of the clay by the trivalent Ce^{3+} ions but also related to the increase of the ionic strength in the clay suspension due to the presence of cerium ions [30]. As the result of hydrolysis reaction of the rare earth cations in aqueous media proposed by Baes and Mesmer [35] ($Ce^{3+} + 3H_2O \rightarrow Ce(OH)_3 + 3H^+$), the high cerium concentration doped in clay structure induces an acidification of the solution and also a decrease of pH value. Due to this modification, the CeMMT surface nature becomes less charged than NaMMT and more susceptible to the aggregate formation.

The corrosion protection of CeMMT was characterized by electrochemical impedance spectroscopy and polarization measurements. AA2024 rotating electrode was immersed in chloride electrolyte solution dispersing 0.5% wt. of CeMMT. Fig. 4 shows the Bode plots of AA2024 obtained after 2 h of immersion in the studied solutions.

As it was seen in Fig. 4, cerium modified clay shows a positive effect on the corrosion protection of aluminum alloy 2024. The impedance modulus at low frequency reaches a value of the order of $3 \times 10^4\ \Omega\ cm^2$ in the presence of CeMMT, which is higher than that one obtained from the reference solution. The phase diagram in the case of CeMMT only shows one-time constant, related to a more capacitive behavior than that one obtained for the reference. This behavior seems to be like the one observed from adding free cerium ions to electrolyte solution (Fig. 1), relating to a release of Ce (III) ions from MMT platelets. Based on these electrochemical measurements, it can be calculated that the cerium-modified clays show a high inhibition efficiency (I_{eff} = 96% after 2 h of immersion) in the anticorrosion protection of aluminum 2024 electrode.

Fig. 5 displays the images of the aluminum electrode surface after 2 h of immersion in the studied solutions. Comparing the electrode surface immersed in the reference solution (Fig. 2a), it appears that the unmodified NaMMT cannot protect the AA2024 substrate (Fig. 5a). Furthermore, no accumulation of corrosion products can be observed on electrode surface for the sample immersed in solution containing cerium-modified clay (Fig. 5b). The aluminum surface is protected by a thin layer, which may be due to the precipitation of cerium hydroxide due to the release of Ce (III) ions into the solution [3,16,20,21].

In parallel, the polarization curves were recorded for the AA2024 rotating electrode after 2 h of immersion in these solutions and the curves are presented in Fig. 6. The curves obtained in blank 0.1 M NaCl solution are also considered as reference. The results obtained demonstrate that the addition of Ce^{3+} ions provides an anticorrosion protection for aluminum alloy 2024. After 2 h of immersion of AA2024 rotating electrode in 0.1 M NaCl solution, it is observed that the densities of the anodic and cathodic currents i_{an} and i_{cath}, decrease in the presence of Ce (III) ions compared to those ones obtained for the reference solution. The value of E_{corr} is close to that one obtained without inhibitor. No pitting corrosion is observed on the AA2024 surface after 2 h of exposure in the studied solution. This indicates that Ce^{3+} ions act as mixed inhibitor in the range of studied concentration and for this period of immersion time. In addition, a plateau can be observed on the anodic branch, reflecting a passivation zone on aluminum in presence

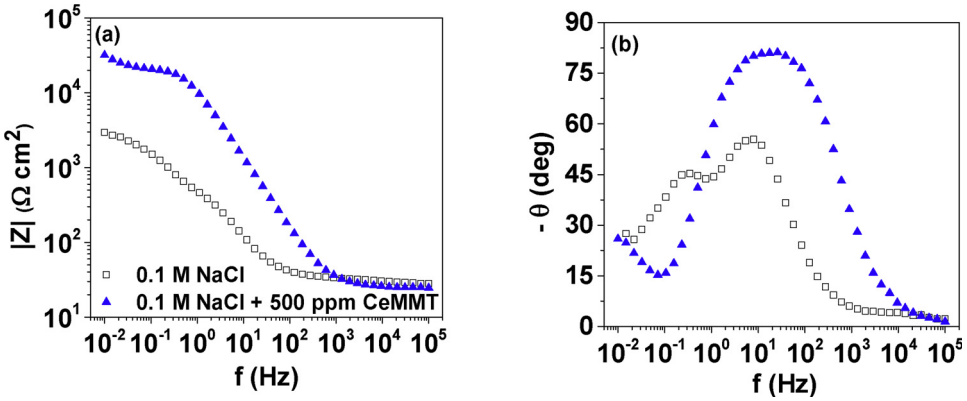

Fig. 4. Bode diagrams of aluminum 2024 rotating electrode after 2 h of immersion in 0.1 M NaCl solution with and without 0.5%wt cerium-modified clay particles: (a) modulus and ((b) phase angle.

of Ce^{3+} ions. In parallel, clays modified with Ce^{3+} ions present an effective capacity in the protection of aluminum alloy 2024. In comparison with the polarization curves obtained for the reference solution, a clear inhibition effect is observed which is attributed to the release of Ce^{3+} ions from the platelets clay to the electrolyte solution. The CeMMT react on the cathodic zones (Fig. 6a), resulting in a decrease of the current density and a shift on the value of E_{corr} (−1 V) towards more negative values than those obtained for reference solution (−0.56 V). In presence of NaMMT, the corrosion current density is as high as the reference system. A corrosion potential shift is observed and is associated to the alkaline pH measured (10.5) when NaMMT are introduced in aqueous solution. It cannot be excluded that this pH increase contributes to the aluminum dissolution and so to a higher corrosion rate.

In order to confirm the release of Ce^{3+} from CeMMT structure into electrolyte solution, the solutions were analyzed by UV–vis analysis after different immersion times in the chloride solution. Fig. 7 displays the UV–vis adsorption spectra of the Ce (III) ions at different selected concentrations and the amount of cerium released from the CeMMT versus immersion time in 0.1 M NaCl solution.

The UV–vis absorbance spectra of cerium (III) in 0.1 M NaCl medium (Fig. 7a) show three peaks in the ultraviolet zone at 237.44 nm, 251.09 nm and 299.03 nm respectively. In agreement with the results presented by Greenhaus et al. [36], the absorbance peak corresponding to the peak around 251.09 nm is chosen to establish a cerium calibration curve. The results presented in Fig. 7b confirm the release of cerium from the structure of modified clays in the aerated solution. The quantity of released cerium increases rapidly when modified clays are added to the measured solution and stabilizes after 1 h. After 6 h, this value increases slightly until 24 h. At the end of test, the amount of released cerium is about 70% (calculated with the amount of cerium ions incorporated in the clay). This result suggests that one part of cerium ions absorbed at the internal layer is still in the clay structure because this interaction is stronger than the interaction between the cerium ions and the external layer [19]. However, this leached rate can protect the aluminum substrate as confirmed by the electrochemical measurements. Based on these promising results, cerium-modified clay CeMMT is selected for incorporation into sol–gel coating in order to protect AA2024 aluminum alloy substrate.

3.3. Characterization of the corrosion protection of sol–gel coating containing CeMMT particles

Fig. 8 shows SEM images of the cross section of the neat silane layer/the silane layer modified with clay particles used to determine the thickness of the coating. As can be seen, the film thickness of undoped sol–gel is about 507 nm with a homogenous surface, Fig. 8a. The sol–gel coating doped with unmodified clay shows a slight increase in the film thickness value (527 nm, Fig. 8b) which is attributed to the doping of clay particles. Due to the dispersion and sonication in as-prepared step, the clay in the sol suspension is found at the intercalated and exfoliated structures, which induce an increase of film thickness and suggest to a barrier protection to the aluminum substrate [30,37]. In addition, the one doped with cerium-modified clay presents higher

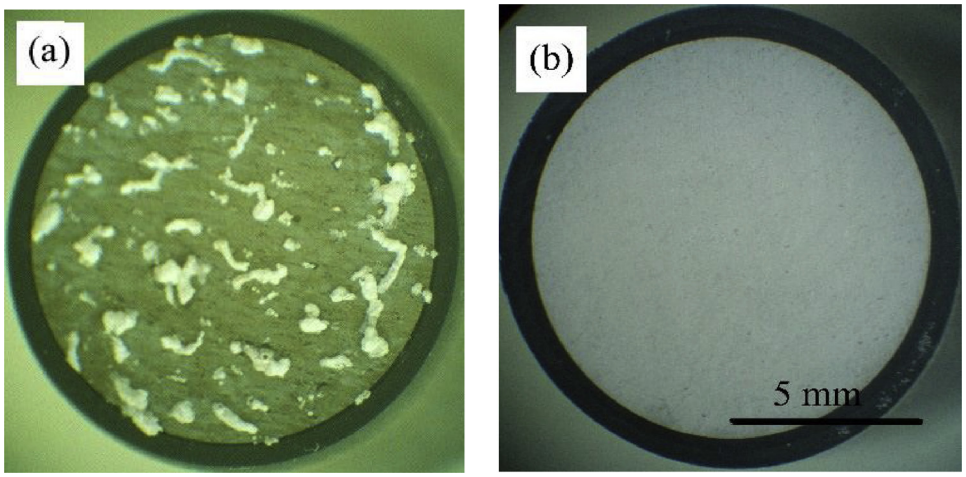

Fig. 5. Optical images of AA2024 rotating electrode after 2 h of immersion (a) in 0.1 M NaCl solution containing 0.5% wt. NaMMT and (b) in 0.1 M NaCl solution containing 0.5% wt.

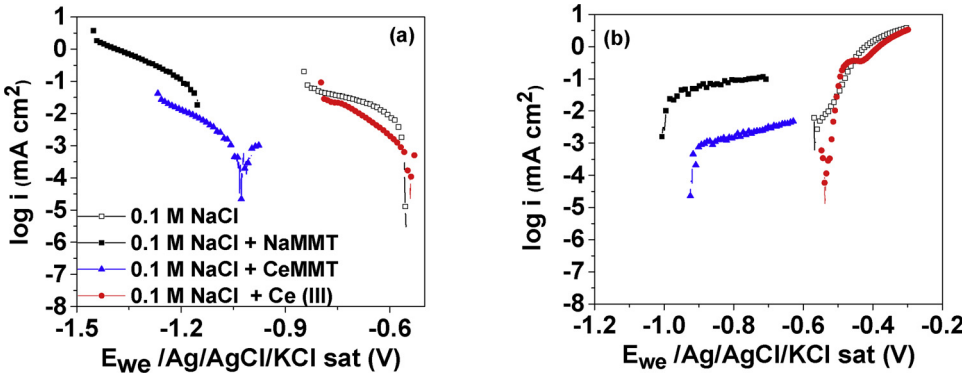

Fig. 6. Cathodic (a) and anodic (b) polarization curves of AA2024 rotating electrode after 2 h of immersion in 0.1 M NaCl solution with and without cerium-modified clay.

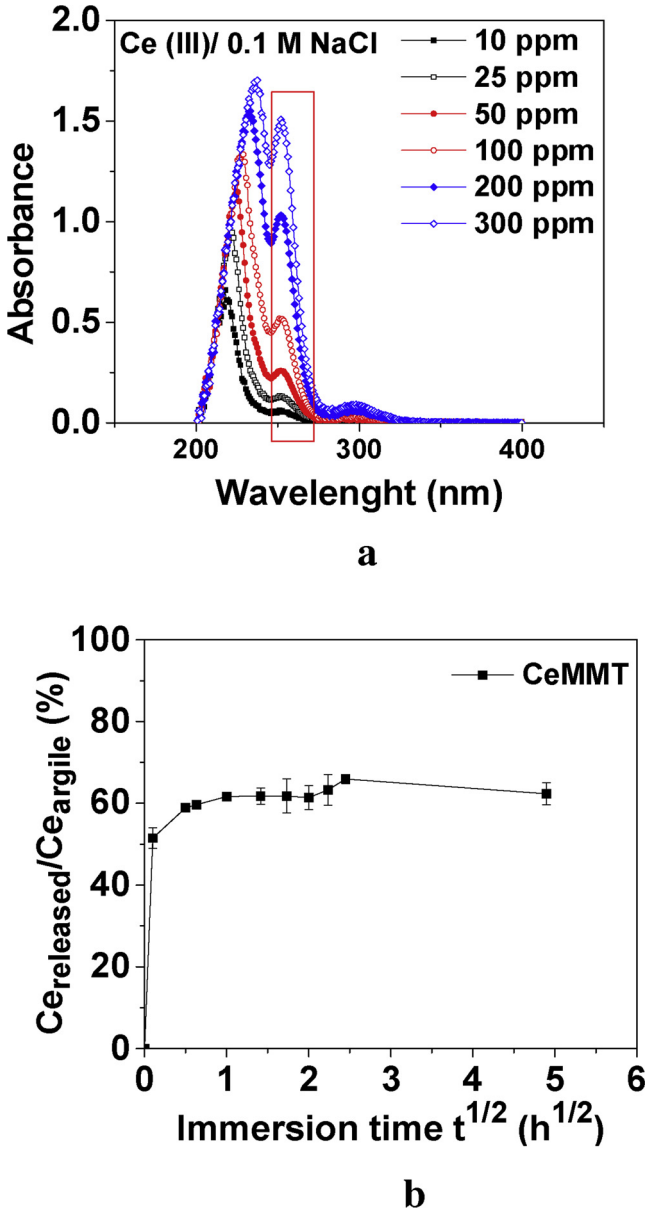

Fig. 7. (a) UV–vis spectra of Ce (III) ions at different concentrations in 0.1 M NaCl solution (b) Released cerium concentration from CeMMT versus immersion time determined by UV–vis analysis.

film thickness value (575 nm, Fig. 8c). The layered structure of clay can also be observed in the cross section in the two cases which confirms the doping of clay in the sol–gel layer.

Fig. 9 represents the Bode diagrams of AA2024 covered with the hybrid sol–gel coating doped with NaMMT or CeMMT after different immersion times in 0.1 M NaCl solution. The Bode diagrams of bare AA2024 after 6 h of immersion in 0.1 M NaCl are also presented as reference. For bare aluminum, the time constant well observed in the phase diagram is related to the alumina layer at the surface, Fig. 9b. The impedance modulus value at low frequency is low, about $2 \times 10^4\ \Omega\,cm^2$. The impedance behavior of aluminum 2024 changes when a hybrid sol–gel coating is deposited on the substrate, Fig. 9a and b respectively. In comparison with the results obtained for bare aluminum 2024, the sol–gel coating provides an improvement of the corrosion protection, marked by an increase of two orders of magnitude of the low frequency impedance modulus. At the short immersion time, the impedance modulus value at low frequency is about $8 \times 10^6\ \Omega\,cm^2$ against $2 \times 10^4\ \Omega\,cm^2$ for bare aluminum. Two-time constants are observed on this phase diagram (Fig. 9b). The time constant at high frequency can be attributed to the presence of a covering and homogenous sol–gel layer as can be observed in the SEM image cross section (Fig. 8a) while the one at low frequency is associated to the interfacial alumina layer due to the presence of Si-O-Al bonds resulting from the interaction between the Si − OH and the Al − OH bonds at the surface [19,37]. During immersion times, the low frequency impedance modulus value gradually decreases, relating to the degradation of the sol–gel film [25,37].

As it is observed in Fig. 9c and d, when the sol–gel layer is doped by using NaMMT, two-time constants are observed in these diagrams: the first one at high frequency linked to silane layer and the second one at low frequency associated with the interface phenomena [19,37]. The presence of NaMMT in sol–gel film changes the global electrochemical behavior with a time constant at high frequency which is strongly depressed compared to the one of the undoped sol–gel at the same immersion time. From 168 h of immersion, this time constant becomes difficult to define which is explained by a strong decrease in the resistance of the silane layer and a modification of the interface. In addition, the impedance modulus value at low frequency is close to $10^7\ \Omega\,cm^2$ at the initial immersion time. These values are close to that one obtained from undoped sol–gel coating, suggesting that the presence of NaMMT maintains barrier properties at the aluminum interface. As can be found in a few publications relating to the introduction of nanoclay into polymer matrix, the good interaction between the OH group of clay platelets and the silanol group promotes the silanization reactions [19,30,35] at the interface. When immersion time increases, the value of the impedance modulus at low frequency gradually decreases, which is due to the degradation of the sol–gel matrix. As a result, water and ions from the electrolyte can easily migrate, resulting in a decrease in the modulus value of doped sol–gel coating [29,31].

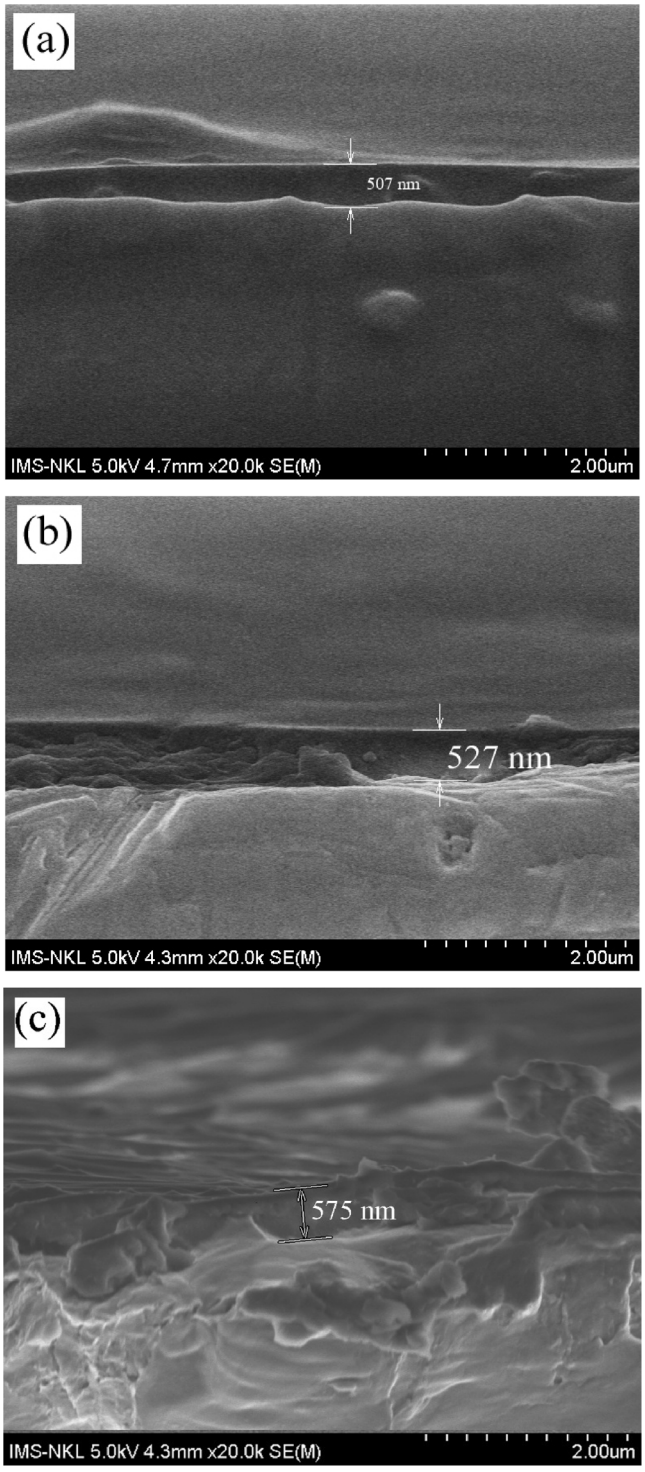

Fig. 8. SEM cross section images of (a) neat sol–gel layer, (b) sol–gel layer doped with un-modified clay NaMMT, (c) sol–gel layer doped with cerium-modified clay CeMMT deposited onto AA2024 substrate.

Results in Fig. 9(e + f) show a modification in electrochemical behavior when Ce (III) ions were inserted in clay structure. It is observed that the first time constant at high frequency is more pronounced than that one observed in the case of NaMMT doped sol–gel (Fig. 9d). So, the sol–gel layer doped with CeMMT is more capacitive than that one doped with un-modified NaMMT. The electrochemical properties, in this case, seem like that ones obtained by the undoped sol–gel coating (Fig. 9a) but indicate a reinforcement of the barrier properties. At the initial immersion time, impedance modulus values at low frequency gradually decreases but remains stable for 24 h of immersion, Fig. 9e respectively. In parallel, the shape of phase diagram changes during immersion time (Fig. 9f). The time constant related to sol–gel layer is gradually depressed while the second time constant increases versus immersion time. This phenomenon can be explained by the role of doped-cerium ions which reinforced the interface of the metallic substrate with time [13,15].

These electrochemical behaviors of sol–gel system can be described by an equivalent electrical circuit (EEC) using ZSim Win 3.50 which is illustrated in Fig. 10. In this case, the pure capacitance C is replaced by the constant phase element Q which is written as $Q = (Q_o^{-1} (i\omega)^{-n})$ where Q_o is the constant phase element admittance and n is a factor variable between 0 and 1. The evolution of electrochemical parameters as a function of immersion time in 0.1 M NaCl solution can be found in Fig. 11.

As observed in Fig. 11, the R_{coat} values of the NaMMT-doped sol–gel film are low, resulting to an alteration of sol–gel layer due to the interactions between the clays and the silanol groups during the hydrolysis [19], (Fig. 11a). On the other hand, the R_{coat} values of the undoped sol–gel film, in this case, are higher, which confirmed that in the case of doped clays, the contribution of the silane layer to the total impedance is less important than the protection related to the interface. In the case of CeMMT-doped sol–gel coating, the film resistance shows a high value which can be related to the high corrosion resistance properties. As comparison, this correlates to the high values of n_{coat} (between 0.91–0.97) which indicated a behavior close to a pure capacitance of the silane film Q_{coat} (Fig. 11b). The coating capacitance obtained for the NaMMT-doped sol–gel film is high (n_{coat} values between 0.84 and 0.87) and its R_{coat} value is low which are related to the lower barrier properties of the sol–gel film [19]. This Q_{coat} value presents an increasing trend indicating a degradation of layer due to penetration of water into the film [31]. The fitting parameters corresponding to the silane sol–gel film indicate that the presence of cerium-modified clay could improve its corrosion resistance. On the other hand, the evolution of fitting parameters corresponding to the alumina layer gives information on the interface silane film/aluminum substrate layer (Fig. 11 c and d). The resistance values (R_{oxide}) of the NaMMT-doped film show a degradation at the beginning of immersion and then present a higher value than non-doped film. Moreover, the evolution of interfacial layer R_{oxide} of CeMMT-doped sol–gel always shows stable values up to the end of measurement and its capacitance Q_{oxide} revealed lowest values compared to the other sol–gel layer suggesting a good protection to the aluminum substrate [38]. The lower value of Q_{oxide} can also be representative of a higher interfacial film thickness relating to the reinforcement due to the cerium ions at the interface [15,19,39]. Nevertheless, in the present case the value of n_{ox} is too low (between 0.58 and 0.63) to confirm a thicker layer.

As it is observed in the evolution of $|Z|_{10mHz}$ values of the various doped sol–gel films (Fig.11e), the modulus values at low frequency obtained for the un-doped sol–gel film progressively decrease up to the end of measurement confirming that the neat sol–gel layer is not sufficient to protect the metallic substrate for long time of immersion [5,9,37]. The same trend is recorded for the low modulus values obtained for the NaMMT-doped sol–gel film from the beginning of immersion but a higher value is measured at the end of test compared to the undoped sol–gel film. This can be attributed to the reinforcement effect given by the presence of clay nanoparticles as mentioned in the literature [19,30]. On the other hand, the modulus values corresponding to the CeMMT-doped coating are higher than the other ones, about 10^7 Ω cm^2 at the beginning of measurement (Fig. 11e). These values progressively decrease following immersion time and then stabilize at a quite stable value of 4×10^6 Ω cm^2. This reinforcement is due to the barrier effect given by the incorporation of cerium-modified clay into the sol–gel formulation and also by the contribution to the reinforcement at the interface by cerium ions doping [15].

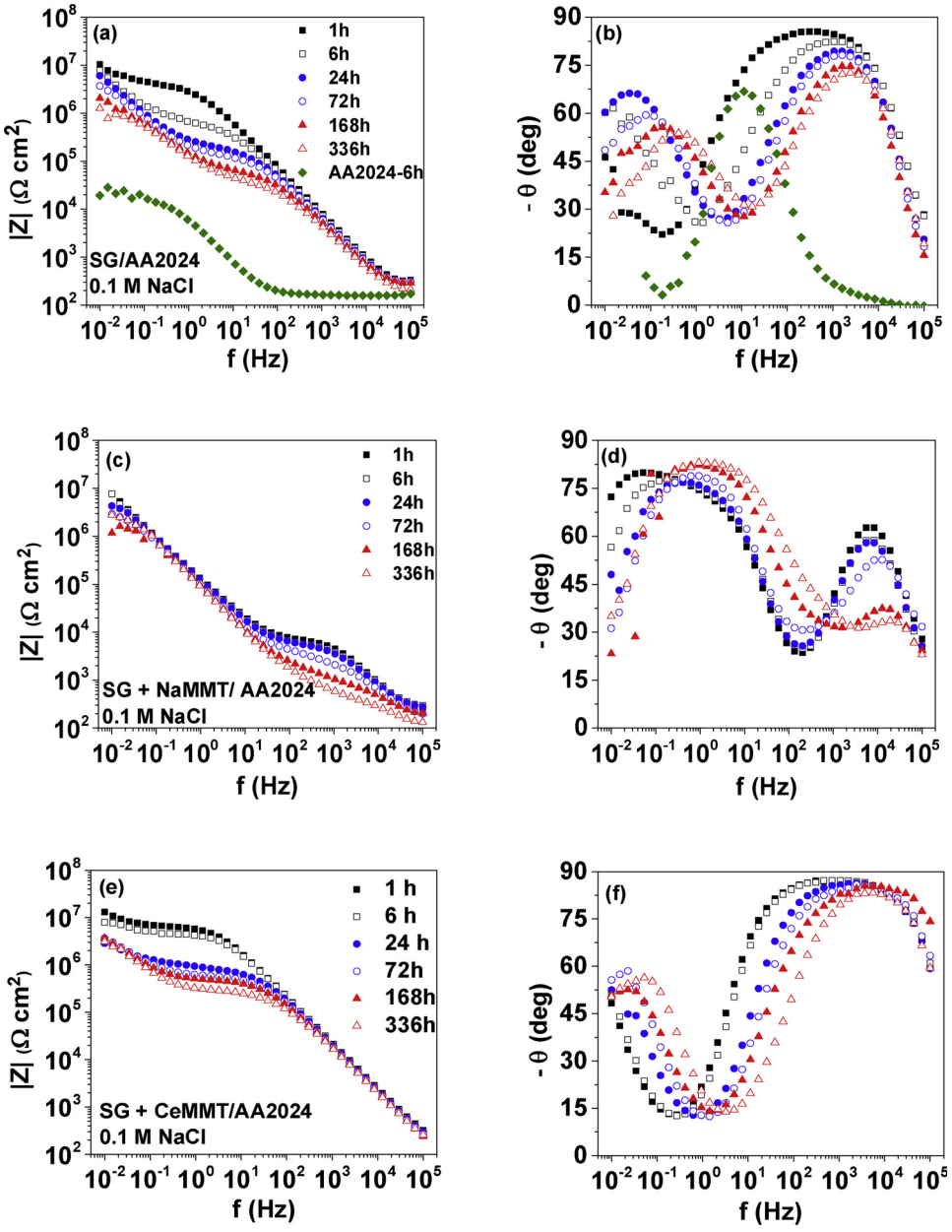

Fig. 9. Bode diagrams of AA2024 samples coated (a + b) with an undoped hybrid sol–gel coating, (c + d) with a hybrid sol–gel doped with 0.5% wt. NaMMT, (e + f) with a hybrid sol–gel doped with 0.5%wt CeMMT (e + f) versus immersion time in 0.1 M NaCl solution.

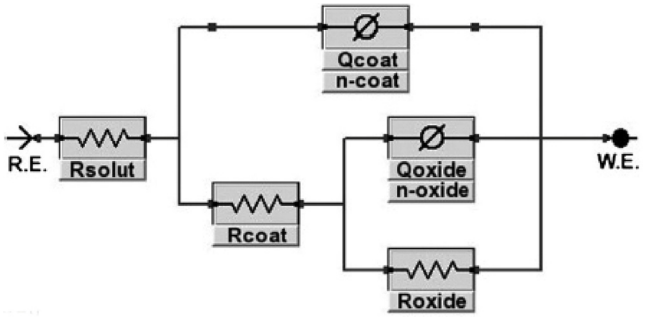

Fig. 10. Equivalent electric circuit (EEC) used for EIS fitting: electrolyte resistance (R_{solut}), coating capacitance (Q_{coat}), sol–gel film resistance (R_{coat}), double layer capacitance (Q_{oxide}) and charge transfer resistance (R_{oxide}).

Fig. 12 shows the surface appearance (Fig.12a–c) of aluminum alloy 2024 coated with sol–gel film or (un) modified clay doped sol–gel films and the microscope image of the artificial scratch (Fig. 12d–f) after 72 h of salt spray test.

As it can be observed, the specimen coated with un-doped sol–gel film dramatically corrodes after 3 days of salt spray test, Fig. 12a, with numerous corrosion products appearing on the surface specimen and around the scratch, Fig. 12d. This phenomenon seems to be limited when the sol–gel film is doped with NaMMT clay, Fig. 12b respectively. The corrosion products still appear on the surface sample with a less important accumulation than for the first case, which is related to the protection effect on the interface due to the incorporation of NaMMT particles. However, for NaMMT-doped sol–gel layer, Fig. 12e, corrosion appears in the scratch revealing a passive protection behavior of un-modified clay particles. On the other hand, the better performance in salt spray test is obtained for the sol–gel coating doped with CeMMT particles. No corrosion products can be obviously observed at the

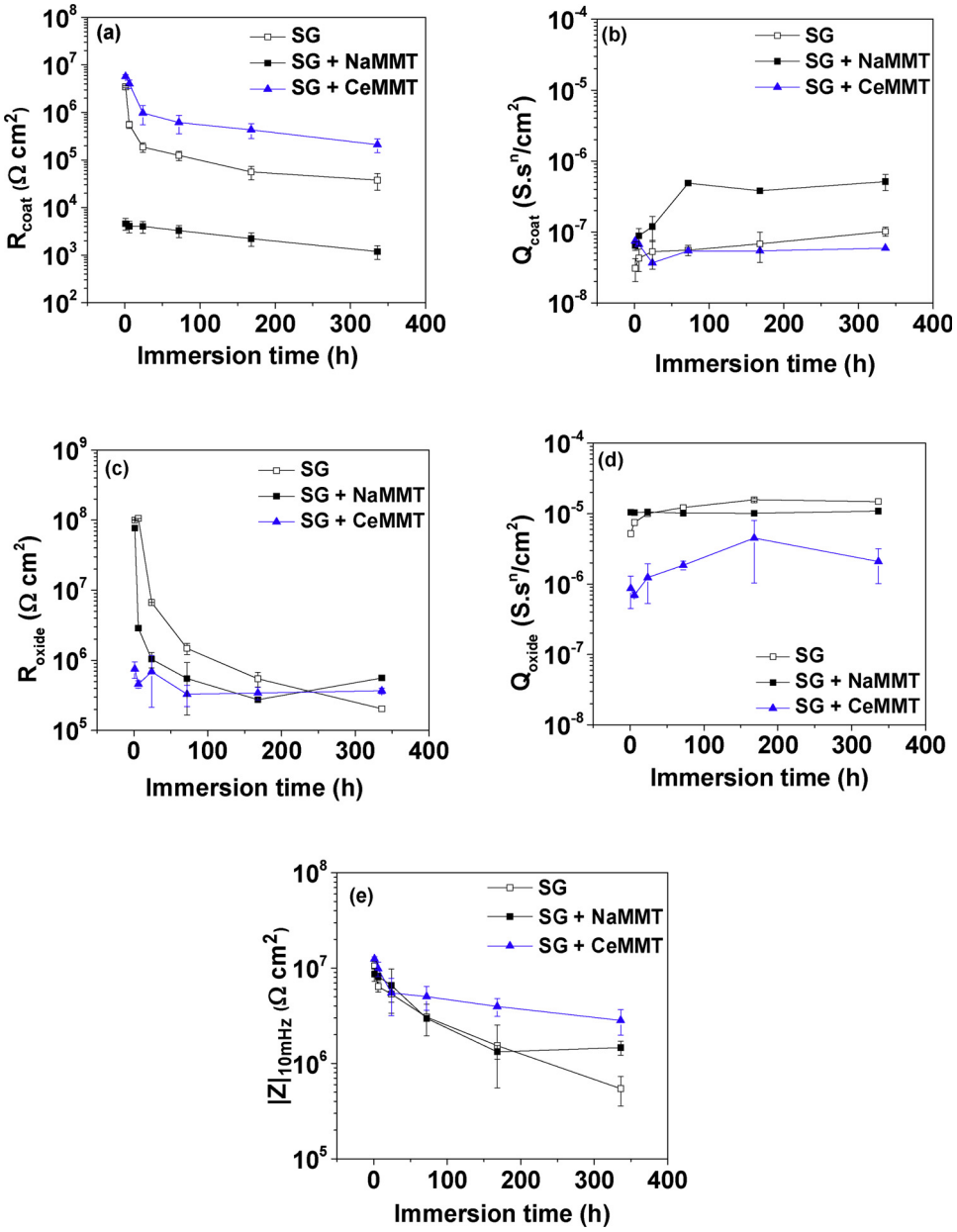

Fig. 11. Evolution of electrochemical parameters of studied systems versus immersion time in 0.1 M NaCl: (a) R_{coat}, (b) Q_{coat}, (c) R_{oxide}, (d) Q_{oxide}, (e) Z_{10mHz}.

surface sample (Fig. 12c). The surface is protected, and only some products can be observed at the artificial scratch (Fig. 12f), which can be related to the formation of cerium hydroxide due to the release of cerium (III) ions [3,16].

4. Conclusions

In this study, a dense, hybrid sol–gel coating formulation was developed. The electrochemical impedance measurements proved the effective passive barrier protection given by this sol–gel layer to protect the metallic substrate. In order to reinforce the anti-corrosion properties and to provide an active protection, the cerium-based inhibitors are then incorporated in this sol–gel formulation by using montmorillonite as a reservoir for Ce (III) ions. At low concentration of cerium-modified clays particles (0.5% wt), it had been shown that cerium– modified clay played a role as effective cathodic inhibitor of aluminum 2024 substrate due to the release of cerium ions in the corrosive medium. The leached cerium rate is about 70% which firstly comes from the cerium ions adhered on the external layer of clay platelets. The incorporation of cerium ions into the clay platelets helps to improve the barrier properties of sol–gel film. Furthermore, the presence of cerium ions at the interface favorizes the formation of cerium hydroxide in order to protect aluminum substrate so the corrosion resistance of sol–gel layer is reinforced. The salt spray test confirms that the cerium- modified clay-doped sol–gel coating provided a positive effect on the protection of the aluminum alloy 2024 in terms of the barrier effect and, also the corrosion inhibition due to the self-healing effect of cerium-based inhibitors.

Conflict of interest

All the authors declare that they have no conflict of interest.

Acknowledgements

The author would like to thank ARES-CCD (Belgium) for their

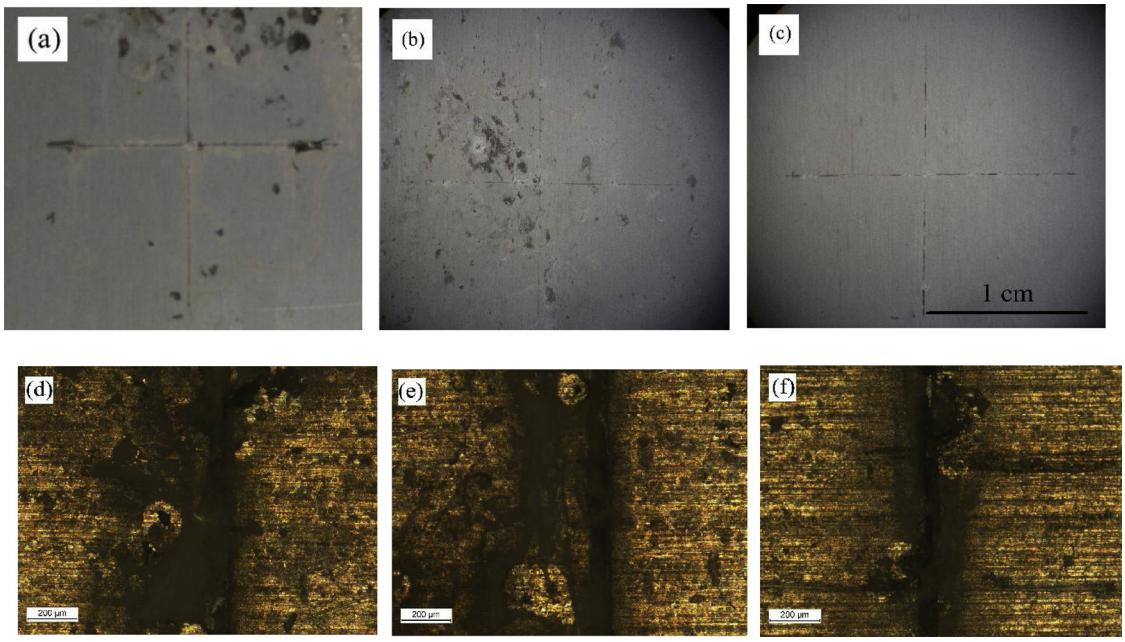

Fig. 12. Optical images of AA2024 surface coated (a + d) with undoped sol–gel film, (b + e) with NaMMT clay doped sol–gel film and (c + f) with CeMMT doped sol–gel film after 72 h of salt spray test.

financial support in the framework of the Research Project (PRD2013-2018) between Institute of Tropical Technology (ITT-VAST, Vietnam) and Materials Science Department (UMONS, Belgium).

References

[1] R.L. Twite, G.P. Bierwagen, Review of alternatives to chrome for corrosion protection of aluminum aerospace alloys, Prog. Org. Coat. 33 (1998) 91–100.
[2] M. Bethencourt, F.J. Botana, J.J. Calvino, M. Marcos, M.A. Rodriguez-Chacon, Lanthanide compounds as environmentally — friendly inhibitors of aluminum alloys: a review, Corros. Sci. 40 (11) (1998) 1803–1819.
[3] E.A. Matter, S. Kozhukharov, M. Machkova, V. Kozhukharov, Comparison between the inhibition efficiencies of Ce(III) and Ce(IV) ammonium nitrates against corrosion of AA2024 aluminum alloy in solutions of low chloride concentration, Corros. Sci. 62 (2012) 22–33.
[4] P. Rodic, I. Milosev, Corrosion Inhibition of pure aluminum and alloys AA2024-T3 and AA7075-T6 by Cerium (III) and Cerium (IV) salts, J. Electrochem. Soc. 163 (3) (2016) C85–C93.
[5] H. Shi, F. Liu, E. Han, Corrosion behaviour of sol–gel coatings doped with cerium salts on 2024-T3 aluminum alloy, Mater. Chem. Phys. 124 (2010) 291–297.
[6] R. Naderi, M. Fedel, F. Deflorian, M. Poelman, M.-G. Olivier, Synergistic effect of clay nanoparticles and cerium component on the corrosion behavior of eco-friendly silane sol–gel layer applied on pure aluminum, Surf. Coat. Technol. 224 (2013) 93–100.
[7] R.V. Lakshmi, S.T. Aruma, S. Sampath, Ceria nanoparticles vis-à-vis cerium nitrate as corrosion inhibitors for silica-alumina hybrid sol–gel coating, Appl. Surf. Sci. 393 (2017) 397–404.
[8] K.A. Yasakau, M.L. Zheludkevich, O.V. Karavai, M.G.S. Ferreira, Influence of inhibitor addition on the corrosion protection performance of sol–gel coatings on AA2024, Prog. Org. Coat. 63 (2008) 352–361.
[9] M. Schem, et al., CeO_2-filled sol–gel coatings for corrosion protection of AA2024-T3 aluminum alloy, Corros. Sci. 51 (2009) 2304–2315.
[10] M.F. Montemor, R. Pinto, M.G.S. Ferreira, Chemical composition and corrosion protection of silane films modified with CeO_2 nanoparticles, Electrochim. Acta 54 (2009) 5179–5189.
[11] M.F. Montemor, W. Trabelsi, M.L. Zheludkevich, M.G.S. Ferreira, Modification of bis-silane with rare-earth cations for improved corrosion protection of galvanized steel substrates, Prog. Org. Coat. 57 (2006) 67–77.
[12] P.H. Suegama, H.G. de Melo, A.V. Benedetti, I.V. Aoki, Influence of cerium (IV) ions on the mechanism of organosilane polymerization and on the improvement of its barrier properties, Electrochim. Acta 54 (2009) 2655–2662.
[13] M.-E. Druart, I. Recloux, T.T. Thai, S. Ershov, R. Snyders, M.-G. Olivier, Impact of the addition of cerium salts (Ce(III) and Ce(VI) on formation and aeging of a silica sol–gel layer, Surf. Coat. Technol. 304 (2016) 40–50.
[14] U. Tiringer, B. Music, D. Zimerl, G. Sekularac, S. Stavber, The effects of cerium ions on the curing, polymerisation and condensation of hybrid sol–gel coatings, J. Non-Cryst. Solids 510 (2019) 93–100.
[15] M. Fedel, E. Callone, M. Fabbian, F. Deflorian, S. Diré, Influence of Ce^{3+} doping on molecular organization of Si-based organic/inorganic sol–gel layers for corrosion protection, Appl. Surf. Sci. 414 (2017) 82–91.
[16] V. Palanivel, Y. Huang, W.J. Van Ooij, Effects of addition of corrosion inhibitors to silane films on the performance of AA2024-T3 in a 0.5M NaCl solution, Prog. Org. Coat. 53 (2005) 153–168.
[17] A.T. Trinh, et al., Improvement of adherence and anticorrosion properties of an epoxy-polyamide coating on steel by incorporation of an indole-3 butyric acid-modified nanomagnetite, J. Coat. Technol. Res. 13 (3) (2016) 489–499.
[18] I.A. Kartsonakis, et al., Multifunctional epoxy coatings combining a mixture of traps and inhibitor loaded nanocontainers for corrosion protection of AA2024-T3, Corros. Sci. 85 (2014) 147–159.
[19] C. Motte, M. Poelman, A. Roobroeck, M. Fedel, F. Deflorian, M.-G. Olivier, Improvement of corrosion protection offered to galvanized steel by incorporation of lanthanide modified nanoclays in silane layer, Prog. Org. Coat. 74 (2012) 326–333.
[20] L. Rassouli, R. Naderi, M. Mahdavain, Study of the impact of sequence of corrosion inhibitor doping in zeolite on the self-healing properties of silane sol–gel film, J. Ind. Eng. Chem. 66 (2018) 221–2230.
[21] M.A. Zadeh, J. Tedim, M. Zheludkevich, S. van der Zwaag, S.J. Garcia, Synergetic active corrosion protection of AA2024-T3 by 2D-anionic and 3D-cationic nanocontainers loaded with Ce and mercaptobenzothiazole, Corros. Sci. 135 (2018) 35–45.
[22] S.S. Ray, M. Okamoto, Polymer/layered silicate nanocomposites: a review from preparation to processing, Prog. Polym. Sci. 28 (2003) 1539–1641.
[23] S. Pavlidou, C.D. Papaspyrides, A review on polymer-layered silicate nanocomposites, Prog. Polym. Sci. 33 (2008) 1119–1198.
[24] J. Konta, Clay and man: clay raw materials in the service of man, Appl. Surf. Sci. 10 (1995) 275–335.
[25] F. Deflorian, S. Rossi, M. Fedel, C. Motte, Electrochemical investigation of high-performance silane sol–gel films containing clay nanoparticles, Prog. Org. Coat. 69 (2010) 158–166.
[26] A.T. Trinh, et al., 8-hydroxyquinoline-modified clay incorporated in an epoxy coating for the corrosion protection of carbon steel, Surf. Interfaces 14 (2019) 26–33.
[27] M. Fedel, E. Callone, S. Diré, F. Deflorian, M.-G. Olivier, M. Poelman, Effect of Na-Montmorillonite sonication on the protective properties of hybrid silica coatings, Electrochim. Acta 124 (2014) 90–99.
[28] P.C. Suarez-Martinez, J. Robinson, H. An, R.C. Nahas, D. Cinoman, J.I. Lutkenhaus, Polymer-clay nanocomposite coatings as efficient, environment-friendly surface pretreatments for aluminum alloy 2024-T3, Electrochim. Acta 260 (2018) 73–81.
[29] E. Darmiani, I. Danaee, G.R. Rashed, D. Zaarei, Formulation and study of corrosion prevention behavior of epoxy cerium nitrat-montmorillonite nanocomposite coated carbon steel, J. Coat. Technol. Res. 10 (4) (2013) 493–502.
[30] M.-G. Olivier, et al., Study of the effect of nanoclay incorporation on the rheological properties and corrosion protection by a silane layer, Prog. Org. Coat. 72 (2011) 15–20.
[31] N. Asadi, R. Naderi, M. Saremi, Determination of optimum concentration of cloisite in an eco-friendly silane sol–gel film to improve corrosion resistance of mild steel, Appl. Clay Sci. 95 (2014) 243–251.
[32] T.T. Thai, M.-E. Druart, Y. Paint, A.T. Trinh, M.-G. Olivier, Influence of the sol–gel mesoporosity on the corrosion protection given by an epoxy primer applied on alunium alloy 2024-T3, Prog. Org. Coat. 121 (2018) 53–63.
[33] L. Paussa, F. Andreatta, N.C. Rosero Navarro, A. Duran, L. Fedrizzi, Study of the

effect of cerium nitrate on AA2024-T3 by means of electrochemical micro-cell technique, Electrochim. Acta 70 (2012) 25–33.
[34] F. Deflorian, M. Fedel, S. Rossi, P. Kamarchik, Evaluation of mechanically treated cerium (IV) oxides as corrosion inhibitors for galvanized steel, Electrochim. Acta 56 (2011) 7833–7844.
[35] C.F. Baes, R.E. Mesmer, The hydrolysis of cations, J. Chem. Educ. 54 (10) (1977) A429.
[36] H.L. Greenhaus, A.M. Feibush, L. Gordon, Ultraviolet spectrophotometric determination of cerium (III), Anal. Chem. 29 (10) (1957) 1531–1534.
[37] V. Dalmoro, J.H.Z. dos Santos, E. Armelin, C. Alemán, D.S. Azambuja, Sol–gel hybrid film based on organosilane and montmorillonite for corrosion inhibition of AA2024, J. Colloid Interface Sci. 426 (2014) 308–313.
[38] I. Recloux, et al., Optimization of synthesis parameters of mesoporous silica sol–gel thin films for application on 2024 aluminum alloy substrates, Appl. Surf. Sci. 277 (2013) 201–210.
[39] M.F. Montemor, M.G.S. Ferreira, Cerium salt actived nanoparticles as fillers for silane films: evaluation of the corrosion inhibition performance on galvanised steel substrates, Electrochim. Acta 52 (2007) 6976–6987.